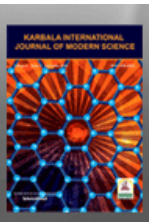

Karbala International Journal of Modern Science

Volume 6 | Issue 3 Article 11

Heat and mass transfer of MHD Casson nanofluid flow through a porous medium past a stretching sheet with Newtonian heating and chemical reaction

Lipika Panigrahi
Veer Surenrda Sai University of Technology, Burla, India

Jayaprakash Panda
Veer Surenrda Sai University of Technology, Burla, India

Kharabela Swain
Gandhi Institute For Technology, Bhubaneswar, India, kharabela1983@gmail.com

Gouranga Charan Dash
Siksha 'O' Anusandhan (Deemed to be University), Bhubaneswar, India

Recommended Citation

Panigrahi, Lipika; Panda, Jayaprakash; Swain, Kharabela; and Dash, Gouranga Charan (2020) "Heat and mass transfer of MHD Casson nanofluid flow through a porous medium past a stretching sheet with Newtonian heating and chemical reaction," *Karbala International Journal of Modern Science*: Vol. 6 : Iss. 3 , Article 11.
Available at: https://doi.org/10.33640/2405-609X.1740

Heat and mass transfer of MHD Casson nanofluid flow through a porous medium past a stretching sheet with Newtonian heating and chemical reaction

Abstract

An analysis is made to investigate the effect of inclined magnetic field on Casson nanofluid over a stretching sheet embedded in a saturated porous matrix in presence of thermal radiation, non-uniform heat source/sink. The heat equation takes care of energy loss due to viscous dissipation and Joulian dissipation. The mass transfer and heat equation become coupled due to thermophoresis and Brownian motion, two important characteristics of nanofluid flow. The convective terms of momentum, heat and mass transfer equations render the equations non-linear. This present flow model is pressure gradient driven and it is eliminated with the help of potential/ambient flow condition. Surface condition is characterised by Newtonian heating/cooling. The numerical solution by Runge-Kutta method with shooting technique results in important findings: formation of inverted boundary layer is to be regulated by adjusting the relative shearing effect of plate and free stream, increase in angle of inclination and thermal radiation ascribe to low flow rate and higher thermal diffusion, in presence of Newtonian heating at the bounding surface the temperature of the nanofluid decreases with the higher values of Casson fluidity; this may have a therapeutic application to control the temperature of blood or any biological fluid.

Keywords

Casson nanofluid, thermal radiation, Newtonian heating/cooling, chemical reaction, non-uniform heat source/sink

Cover Page Footnote

The authors acknowledge their sincere thanks to the honorable unknown referees for their valuable comments.

1. Introduction

The boundary layer flow over a stretching/shrinking sheet has many usages in various manufacturing/industrial processes such as paper production, extraction of polymer sheets, wire coating, etc. The flow and heat transfer due to stretching sheet of an incompressible fluid have several engineering applications such as polymer processing, cooling of electronic devices, and blood flow problems etc. Ibrahim and Shankar [1] studied the flow and heat transfer of a nanofluid past a permeable stretching sheet with slip boundary conditions. Bhukta et al. [2] considered the effect of non-uniform heat source/sink on MHD mixed convection flow over a stretching sheet. Ahmed [3] explored the impact of slip flow analysis of Casson nanofluid over a stretching sheet with chemical reaction. Moreover, investigations are enriched on flow of Casson nanofluid over stretching sheet on different fluid models by Mustafa and Khan [4], Hayat et al. [5], Afify [6] and Abd EI-Aziz et al. [7].

To enhance the thermal conductivity of common fluids, such as water and ethylene glycol etc., nanoparticles (metals/metallic oxide) are mixed with a base fluid to enhance the thermal transport of the nanofluid, which increases the rate of heat transfer. This is due to the higher thermal conductivity of the nanoparticles and associated Brownian motion. Rahman and Eltayeb [8] have examined the effect of thermal radiation on hydromagnetic nanofluid flow. Ibrahim [9] studied the stagnation point flow of nanofluid past a stretching sheet. Swain et al. [10] have observed the impact of non-uniform heat source/sink and viscous dissipation on MHD Williamson nanofluid. They have considered linear/non-linear stretching sheet in their study. Goyal and Bhargava [11] and Seth et al. [12] have studied nanofluid flow over an inclined stretching sheet. Yadav et al. [13−15] have contributed significantly to enrich the literature on nanofluid convection. Further, they studied the transient Soret driven MHD convection flow with nanoparticle suspension. They also accounted for Hall current flow through porous medium. Yadav and Lee [16] considered the MHD nanofluid convection with Hall current effect. Further, the surge of interest of Yadav [17,18] laid the author to work on nanofluid flow in an isotropic/anisotropic medium with rotation and variable gravity in presence of non-uniform heating and chemical reaction.

Casson fluid is a non-Newtonian (visco-inelastic) fluid with yield stress which represents blood flow in narrow arteries. When blood flows from larger diameter arteries at high shear rates it shows Newtonian character. But it exhibits non-Newtonian behaviour when it flows through small diameter arteries at low shear rates (Rathod and Tanveer [19]). Also, viscosity of blood is found to increase at low rates of shear as the red blood cells tend to aggregate into the Rouleaux form. This non-Newtonian behaviour of blood flow presents a flattened parabolic velocity profile rather than the parabolic velocity profile of a Newtonian fluid. The non-Newtonian characteristic is due to yield stress. The yield stress values for normal human blood is between 0.01 and 0.06 dyn/cm^2 (Krishnan et al. [20]). The blood flow in narrow arteries at low shear rates represents Casson fluid characteristics (Blair [21]). Further, Casson [22] studied the validity of Casson fluid model in his studies relating to the flow of blood and observed that at low shear rates the yield stress for blood is nonzero. Such analysis of Merrill et al. [23] supports the Casson fluid model of blood flow in tubes with the diameter of 130−1000 m. The Casson fluid model representing blood flow through narrow arteries at low shear rate is well supported by the experiment made by Charm and Kurland [24]. Chaturani and Samy [25] examined the pulsatile flow of Casson fluid through stenosed arteries using the perturbation method. Madhu and Kishan [26] have considered the flow over a wedge. Kalaivanan et al. [27] have considered the MHD flow Casson nanofluid inspired by aligned magnetic field. Jain and Parmar [28] and Ganga et al. [29] have examined the slip flow of Casson fluid over a stretching sheet. Several authors [30−34] have studied the effects of thermal radiation and chemical reaction on MHD Casson fluid over stretching/shrinking sheets. Recently, Senapati et al. [35] have numerically investigated the Casson nanofluid flow over a stretching sheet.

Hayat et al. [36] studied the nanofluid flow over a stretching surface with Newtonian heating. Uddin et al. [37] considered the influences of Newtonian heating and thermal radiation on boundary layer flow of nanofluid over a stretching sheet through a porous medium. Ahmad et al. [38] examined the Casson nanofluid flow past a wedge considering Newtonian heating. Ullaha et al. [39] explored the effect of Newtonian heating on flow of Casson fluid over a

https://doi.org/10.33640/2405-609X.1740

nonlinearly stretching sheet embedded in a porous medium.

In the present paper we have considered the effect of inclined magnetic field whereas [39] have considered transverse magnetic field which can be derived as a particular case of the present paper for $\gamma = 90^0$. Most importantly, they [39] have considered the free stream velocity as well as pressure gradient as zero. The pressure gradient term $-\frac{\partial p}{\partial x} \neq 0$ which has been accounted for with the help of non-zero potential flow $U_\infty(x)$, outside the boundary layer. Moreover, consideration of additional mechanisms of fluid particle slip during convection of nanofluids contributed to thermophoresis and Brownian diffusion effects as $\frac{D_T}{T_\infty}\left(\frac{\partial T}{\partial y}\right)^2$ and $D_B\frac{\partial C}{\partial y}\frac{\partial T}{\partial y}$ respectively (Boungiorno [40]) which are taken care of in the present discussion. Further [39], have not considered the energy losses due to thermal radiation, viscous dissipation, and Joulian dissipation in heat equation but the present study also takes interest of those losses. Moreover, they have considered only Casson fluid. The present study focuses on nanofluid flow with thermophoresis and Brownian diffusion. In boundary conditions, they have considered the velocity slip at the plate whereas in the present case the plate is subjected to a linear stretching along x-direction $(U_w(x) = ax)$. The additional boundary condition $D_B\frac{\partial C}{\partial y} + \frac{D_T}{T_\infty}\frac{\partial T}{\partial y} = 0$, is due to Brownian diffusion and thermophoresis effects have been considered in the present study also.

Nanoparticles are found in several organisms. Silver and Fe_3O_4 nanoparticles are found in bacteria. An important aspect is that all the metal nanoparticles can be extracted and resuspended. Thus, this process helps to make large quantities of nanoparticles at less cost. Magnetic nanoparticles are important in ferrofluidics, magnetic refrigeration, information storage and magnetic drug delivery.

The novelty of the present study rests upon the followings. The study takes care of the nanofluid flow with Casson fluid as the base fluid and suspended nanoparticles. The important mechanism such as Brownian diffusion and thermophoresis are taken care of to characterise the nanofluid flow. The inclined magnetic field is a generalised approach to simulate the magnetic lines of force acting at-a-distance. It also includes the case of transverse magnetic field. The flow is subjected to an additional body force due to the presence of porous matrix. The concentration variation of reactive diffusing species is another aspect of the study. Most importantly, the surface condition imposes a Newtonian heating/cooling mechanism considering the conductivity of solid surface and base fluid. Another imposed surface condition takes care of thermo and mass diffusive fluxes. Besides the above criteria, the flow is due to stretching of bounding surface and pressure gradient driven. The objective is to simulate the effect of important parameters on flow, heat and mass transfer phenomena.

2. Mathematical formulation

Consider a steady, two dimensional, incompressible, laminar and electrically conducting Casson nanofluid flow past a stretching sheet along positive x-direction. An inclined magnetic field of strength B_0 sin γ with an acute angle (γ) is applied along y-axis. At $\gamma = 90^0$ the magnetic field acts as a transverse magnetic field. The fluid flow is restricted to $y > 0$ which is caused by the linear stretching of the sheet with velocity $U_w(x) = ax$ from a slit keeping the origin fixed as shown in Fig. 1. The velocity of the ambient fluid layer set to be $U_\infty = bx$. It is assumed that.

- the magnetic Reynolds number of the fluid is very small so that the effect of induced magnetic field is neglected.
- there is no slip between base fluid and the bounding surface.
- the fluid has constant properties and the flow is subjected to constant pressure gradient along x-direction which has been determined by ambient flow velocity.
- the porous medium is homogeneous and fully saturated.
- the base fluid is exposed to metallic or metallic-oxides nanoparticles which contributes a complex heat transfer phenomena.
- the heat transfer takes care of viscous dissipation due to internal resistance, Joule heating due to a resistance to passage of electric current.
- the flow phenomena also considers mass transfer of a chemical reactive species with first order chemical reaction.
- the flow, heat and mass transfer phenomena are subject to boundary conditions such as stretching of bounding surface, Newtonian heating, thermophoresis and Brownian motion.

Under the above assumptions, the MHD boundary layer equations for steady flow of Casson nanofluid following [27,41] are given by

$$\frac{\partial u}{\partial x}+\frac{\partial v}{\partial y}=0, \tag{1}$$

$$u\frac{\partial u}{\partial x}+v\frac{\partial u}{\partial y}=U_\infty\frac{\partial U_\infty}{\partial x}+\upsilon_f\left(1+\frac{1}{\beta}\right)\frac{\partial^2 u}{\partial y^2} - \left(\frac{\sigma {B_0}^2}{\rho_f}sin^2\gamma+\frac{\upsilon_f}{Kp^*}\right)(u-U_\infty), \tag{2}$$

$$u\frac{\partial T}{\partial x}+v\frac{\partial T}{\partial y}=\alpha\frac{\partial^2 T}{\partial y^2}+\tau\left\{D_B\frac{\partial C}{\partial y}\frac{\partial T}{\partial y}+\frac{D_T}{T_\infty}\left(\frac{\partial T}{\partial y}\right)^2\right\} - \frac{1}{(\rho c)_f}\frac{\partial q_r}{\partial y}+\frac{\mu}{(\rho c)_f}\left(1+\frac{1}{\beta}\right)\left(\frac{\partial u}{\partial y}\right)^2 +\frac{\sigma B_0^2(u-U_\infty)^2}{(\rho c)_f}sin^2\gamma+\frac{q'''}{(\rho c)_f}, \tag{3}$$

$$u\frac{\partial C}{\partial x}+v\frac{\partial C}{\partial y}=D_B\frac{\partial^2 C}{\partial y^2}+\frac{D_T}{T_\infty}\frac{\partial^2 T}{\partial y^2}-{K_c}^*(C-C_\infty). \tag{4}$$

The appropriate boundary conditions are

$$\left.\begin{aligned} &u=U_w=ax, v=0, -k\frac{\partial T}{\partial y}=h_f(T_w-T_\infty), D_B\frac{\partial C}{\partial y}+\frac{D_T}{T_\infty}\frac{\partial T}{\partial y}=0 \text{ at } y=0,\\ &u\to U_\infty=bx, T\to T_\infty, C\to C_\infty \text{ as } y\to\infty, \end{aligned}\right\} \tag{5}$$

where $\tau=\frac{(\rho c)_p}{(\rho c)_f}$ is the ratio of the nanoparticle heat capacity to the base fluid heat capacity.

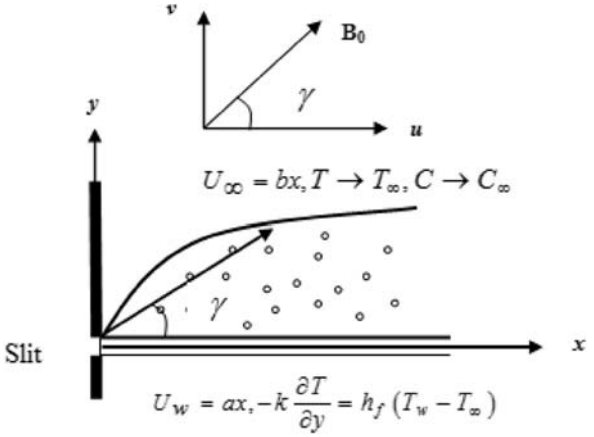

Fig. 1. Flow geometry.

As the plate is subjected to linear stretching we have assumed $u=U_w=ax$ at $y=0$ and $v=0$represents that the plate is impermeable. As the heat flux be transported to the body by the conduction, the following boundary condition holds good.

$$-k\frac{\partial T}{\partial y}=h_f(T_w-T_\infty)$$

Here k is the thermal conductivity of the solid not the fluid at the wall, h_f is the heat transfer coefficient of the fluid [42].

The free stream imposes the balance between the heat flux and mass flux on the bounding surface with thermophoretic diffusion and Brownian motion. Therefore, the free stream condition is self-explanatory as the free stream stretching is subjected to linear stretching and constant temperature and concentration.

Consider the stream function $\psi(x,y)=\sqrt{av_f}xf(\eta)$, such that

$$u=\frac{\partial\psi}{\partial y}, v=-\frac{\partial\psi}{\partial x} \tag{6}$$

and dimensionless similarity transformations

$$\eta=\sqrt{\frac{a}{v_f}}y, \theta(\eta)=\frac{T-T_\infty}{T_w-T_\infty}, \phi(\eta)=\frac{C-C_\infty}{C_w-C_\infty}. \tag{7}$$

Using Rosseland approximation [10], the radiative heat flux q_r is given by

$$q_r=-\frac{4\sigma^*}{3k^*}\frac{\partial T^4}{\partial y}=-\frac{16\sigma^*}{3k^*}T_\infty^3\frac{\partial T}{\partial y}, \tag{8}$$

where σ^* Stefan–Boltzmann constant, k^* is the mean absorption coefficient.

The non-uniform heat source/sink $q'''$is modeled as

$$q'''=\frac{kU_w}{xv_f}[A^*(T_w-T_\infty)f'+B^*(T-T_\infty)], \tag{9}$$

where$A^*$and $B^*$are the coefficients of space and temperature dependent heat source/sink respectively.

Therefore, equation (3) becomes

$$u\frac{\partial T}{\partial x}+v\frac{\partial T}{\partial y}=\alpha\frac{\partial^2 T}{\partial y^2}+\tau\left\{D_B\frac{\partial C}{\partial y}\frac{\partial T}{\partial y}+\frac{D_T}{T_\infty}\left(\frac{\partial T}{\partial y}\right)^2\right\} +\frac{16\sigma^* T_\infty^3}{3k^*(\rho c)_f}\frac{\partial^2 T}{\partial y^2}+\frac{\mu}{(\rho c)_f}\left(1+\frac{1}{\beta}\right)\left(\frac{\partial u}{\partial y}\right)^2 +\frac{\sigma B_0^2(u-U_\infty)^2}{(\rho c)_f}sin^2\gamma+\frac{q'''}{(\rho c)_f}, \tag{10}$$

In view of equations (6) and (7), equations (2), (4), (5) and (10) become

$$\left(1+\frac{1}{\beta}\right)f''' + ff'' - f'^2 + \lambda^2 + \left(M\sin^2\gamma + Kp\right)(\lambda - f') = 0, \tag{11}$$

$$\left(1+\frac{4}{3}R\right)\theta'' + \Pr\left[\begin{array}{l} f\theta' + Nb\theta'\phi' + Nt(\theta')^2 + \\ \left(1+\frac{1}{\beta}\right)Ecf''^2 + EcM\sin^2\gamma f'^2 \end{array}\right] + (A^* f' + B^*\theta) = 0, \tag{12}$$

$$\phi'' + Scf\phi' + \frac{Nt}{Nb}\theta'' - K_c Sc\phi = 0, \tag{13}$$

$$\left.\begin{array}{l} f(\eta) = 0, f'(\eta) = 1, \theta'(\eta) = Bi[\theta(\eta) - 1], Nb\phi'(\eta) \\ \quad + Nt\theta'(\eta) = 0 \ at \\ \eta = 0, \quad f'(\eta) \to \lambda, \theta(\eta) \to 0, \phi(\eta) \to 0 \quad as \quad \eta \to \infty. \end{array}\right\} \tag{14}$$

where $M = \frac{\sigma B_0^2}{a\rho_f}, Kp = \frac{aKp^*}{\upsilon_f}, Sc = \frac{\upsilon_f}{D_B}, \lambda = \frac{b}{a}, \Pr = \frac{\upsilon_f}{\alpha_f}$,

$$R = \frac{4\sigma^* T_\infty^3}{kk^*}, Bi = \frac{h_f}{k}\sqrt{\frac{\upsilon_f}{a}},$$

$$Nb = \frac{\tau D_B(C_w - C_\infty)}{\upsilon_f}, Nt = \frac{\tau D_T(T_w - T_\infty)}{\upsilon_f T_\infty}, K_c = \frac{K_c^*}{a},$$

$$Ec = \frac{U_w^2}{c_f(T_w - T_\infty)}.$$

The temperature field is dependent on Biot number (Bi) when heat transfer takes place into the fluid. The Biot number has the same form as the Nusselt number. There is however one significant difference, k in the Biot number is the thermal conductivity of the solid whilst in Nusselt number, k_f is the thermal conductivity of the fluid. The Nusselt number serves as a dimensionless representation of heat transfer coefficient whereas Biot number describes the boundary conditions in a solid body [42].

The surface conditions of practical interest such as the skin friction coefficient, local Nusselt number and local Sherwood number are given by

$$C_f = \frac{\tau_w}{\rho U_w^2} \Rightarrow C_f\sqrt{\mathrm{Re}_x} = \left(1+\frac{1}{\beta}\right)f''(0),$$

$$Nu_x = \frac{xq_w}{k_f(T_w - T_\infty)} \Rightarrow \frac{Nu_x}{\sqrt{\mathrm{Re}_x}} = -\left(1+\frac{4}{3}R\right)\theta'(0),$$

$$Sh_x = \frac{xq_m}{D_B(C_w - C_\infty)} \Rightarrow \frac{Sh_x}{\sqrt{\mathrm{Re}_x}} = -\phi'(0),$$

where wall shear stress $\tau_w = \mu_f\left(\frac{\partial u}{\partial y}\right)_{y=0}$, wall heat flux $q_w = -k_f\left(\frac{\partial T}{\partial y}\right)_{y=0} + (q_r)_{y=0}$, wall mass flux $q_m = -D_B\left(\frac{\partial C}{\partial y}\right)_{y=0}$, and $\mathrm{Re}_x = \frac{U_w x}{\upsilon_f}$ is the local Reynolds number.

3. Results and discussion

The dimensionless coupled nonlinear ordinary differential equations 11–14 are solved numerically by Runge-Kutta fourth order method with shooting technique using MATLAB code with step length $\Delta\eta = 0.01$and the error tolerance10^{-5}. In this method, the equations are reduced to a set of first order differential equations:

$$y_1' = y_2,$$

$$y_2' = y_3,$$

$$y_3' = \left(\frac{-\beta}{1+\beta}\right)\left[y_1 y_3 - y_2^2 + \lambda^2 + \left(M\sin^2\gamma + Kp\right)(\lambda - y_2)\right]$$

$$y_4' = y_5,$$

$$y_5' = \left(\frac{-3}{3+4R}\right)\left[\Pr\left\{\begin{array}{l} y_1 y_5 + Nby_5 y_7 + Nty_5^2 + \\ \left(1+\frac{1}{\beta}\right)Ecy_3^2 + EcM\sin^2\gamma y_2^2 \end{array}\right\} + A^* y_2 + B^* y_4\right],$$

$$y_6' = y_7,$$

with the initial conditions

$$y_7' = -\left[Scy_1y_7 + \frac{Nt}{Nb}\left(\frac{-3}{3+4R}\right)\left[\Pr\left\{ \begin{array}{l} y_1y_5 + Nby_5y_7 + Nty_5^2 + \\ \left(1+\frac{1}{\beta}\right)Ecy_3^2 + EcM\sin^2\gamma y_2^2 \end{array} \right\} + A^*y_2 + B^*y_4 \right] - K_cScy_6 \right],$$

$$y_1(0)=0, y_2(0)=1, y_4(0)=\frac{Bi+y_5(0)}{Bi}, y_7(0) = \frac{Nt}{Nb}y_5(0).$$

Now, the initial value problem is solved by appropriately guessing the missing initial values i.e. $y_3(0), y_5(0)$, and $y_6(0)$ as $-1.0, -0.5$ and 0.1 respectively using shooting technique for various sets of parameters. There is an inbuilt self corrective procedure in the MATLAB coding to correct the unknown guess values. During calculation we fix the parameters as $\Pr = 10, Sc = 5, \gamma = 60^0, R = Nt = 0.3, M = Kp = \lambda = \beta = Nb = K_c = 0.5, A^* = B^* = Bi = Ec =$ 0.1 unless otherwise the values are mentioned. A comparison is made with previously published works of Mahapatra and Gupta [43] and Ibrahim et al. [44] as shown in Tables 1 and 2. It is found that our numerical results are in excellent agreement.

Fig. 2 exhibits the effects of two important parameters such asβ (Casson fluid parameter exhibiting the rheological property) and λ (the ratio of stretching velocity of free stream and lower plate). It is seen that when stretching rate of free stream exceeds to that of lower plate$(\lambda > 1)$, an increase in β accelerates the velocity contributing to slightly thicker boundary layer. On the other hand, for$\lambda < 1$, the inverted boundary layer symmetrical to $\lambda =$ 1(equality of stretching rates) is being exhibited with opposite affect causing a flow reversal. The reason of this flow characteristic can be attributed to over powering of shearing effects between plate and free stream. Consequently, momentum transport between the layers adjacent to free stream and solid surface gets altered.

Fig. 3 shows the effects of permeability of the isotropic medium (Kp) and resistive electromagnetic force, known as viscous breaking force (M). For isotropic medium permeability Kp is a scalar otherwise it is a second order tensor and it depends upon the geometry of the medium and its dimension is$(\text{length})^2$. It is observed that an increase in $Kp$and M gives rise to low flow rates. The reason is trivial due to additional resistive forces. From Fig. 4 it is seen that an increase in the angle of inclination(γ) decreases the velocity. The same effect is observed by Ref. [27]. Since sin γ is an increasing function when$0 < \gamma < 90^0$, the strength of magnetic field $B_0 \sin\gamma$ also increases. It is further observed that an increase in Casson parameter (β) decreases the velocity as higher values of βlead to decrease the yield stress.

Fig. 5 depicts the variation of thermal boundary layers i.e. the layers depicting the transfer of thermal energy between the no slip and free stream. The higher values ofPr, reduce the rate of heat transfer since it contributes to low heat conductivity. The effect of radiation parameter (R) is to increase the thermal energy transport significantly contributing to thicker thermal boundary layer as it accelerates the process of diffusion of thermal energy across the layers. This phenomenon ascribes to higher thermal diffusion.

Table 1
Comparison of $f''(0)$ for various values of $\lambda$when.$M = Kp = Nt = A^* = B^* = Sc = Ec = Kc = Nb = 0, \beta \to \infty$.

λ	Mahapatra and Gupta [43]	Ibrahim et al. [44]	Present results
0.1	−0.9694	−0.9694	−0.969385
0.2	−0.9181	−0.9181	−0.918106
0.5	−0.6673	−0.6673	−0.667263
2.0	2.0175	2.0175	2.017501
3.0	4.7293	4.7292	4.729277

Table 2
Comparison of $-\theta'(0)$ for various values of $\lambda$and Pr when.$Kp = Nt = A^* = B^* = Sc = Ec = Kc = Nb = 0, \beta \to \infty$.

Pr	λ	Ibrahim et al. [44]	Present results
1.0	0.1	0.6022	0.602157
	0.2	0.6245	0.624468
	0.5	0.6924	0.692449
1.5	0.1	0.7768	0.776800
	0.2	0.7971	0.797122
	0.5	0.8648	0.864794

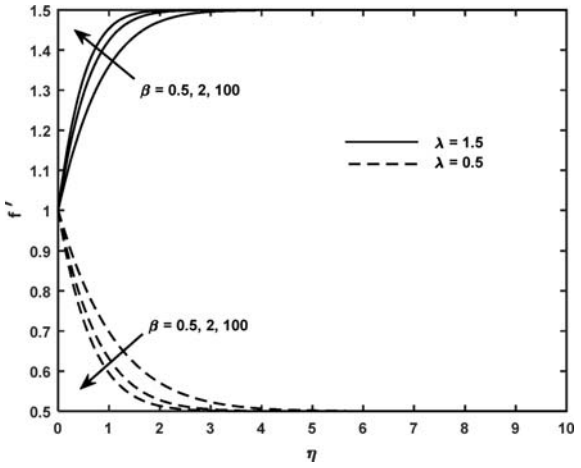

Fig. 2. Velocity profiles for different values λ and β

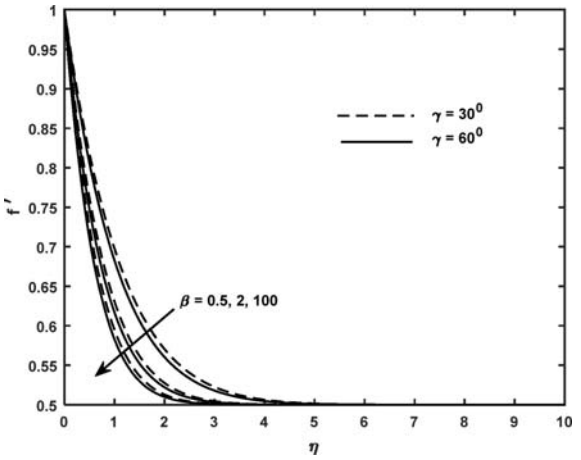

Fig. 4. Velocity profiles for different values of β and γ

Figs. 6 and 7 show the effects of Casson parameter(β), angle of inclination(γ) and Biot number(Bi). It represents the heat conduction at the interface solid surface as well as fluid medium for $Bi > 0$(Newtonian cooling) and $Bi < 0$(Newtonian heating) cases. From Fig. 6 it is observed that the higher rate of Newtonian cooling increases the temperature of the fluid. It is seen that the increasing values of angle of inclination(γ) increase the temperature profile as observed by Ref. [27]. Further, temperature enhances with the increasing values of Casson parameter(β). The same result is obtained in the present study($Bi > 0$, Newtonian cooling) and [39] but the present study reveals that in presence of Newtonian heating ($Bi < 0$)and Casson parameter (β)decreases the temperature (Fig. 7). Since the plate gets heated, the thermal energy is drawn from the fluid mass resulting fall of temperature. This case was not studied in earlier published works. Thus, it is concluded that in presence of Newtonian heating at the bounding surface, the temperature of the nanofluid decreases with the higher values of Casson fluidity. This may have a therapeutic application to control the temperature of blood or any biological fluid. Further, by comparing the present work with that of [39] temperature increases as Biot number increases.

Fig. 8 reveals the effects of space dependent heat source/sink (A^*) and temperature dependent heat source/sink(B^*). The higher values of $A^*$and B^* enhance the temperature in all the layers contributing

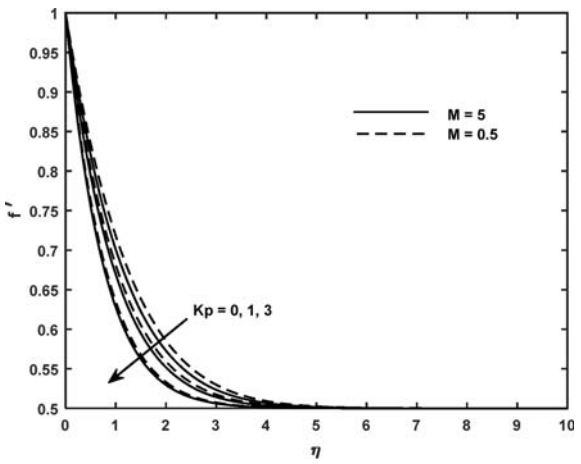

Fig. 3. Velocity profiles for different values M and Kp

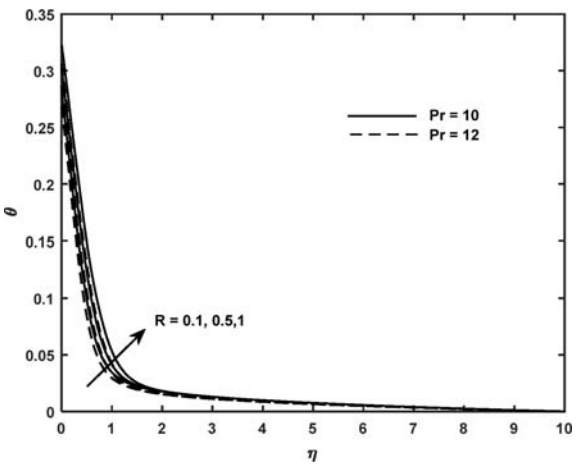

Fig. 5. Temperature profiles for different values of R and Pr

to thicker thermal boundary layer. Fig. 9 exhibits the effects of Eckert number $(Ec)$and thermophoresis parameter(Nt). It is seen that both EcandNt, contribute to rise in temperature distribution. The reason is trivial. The Eckert number is interpreted as the addition of heat due to viscous dissipation. Similarly, Nt depends on thermal diffusivity as well as difference of temperature between wall and ambient state. Hence, an increase in Nt enhances the temperature also.

Fig. 10 shows the concentration level depletes with higher rate of destructive reaction $(K_c > 0)$ as well as for low Schmidt number (Sc) i.e. for lighter diffusing species $(Sc = 5)$ otherwise for higher values of Sc it increases. Fig. 11 depicts the effects of Brownian motion (Nb) and thermophoresis parameter(Nt). The

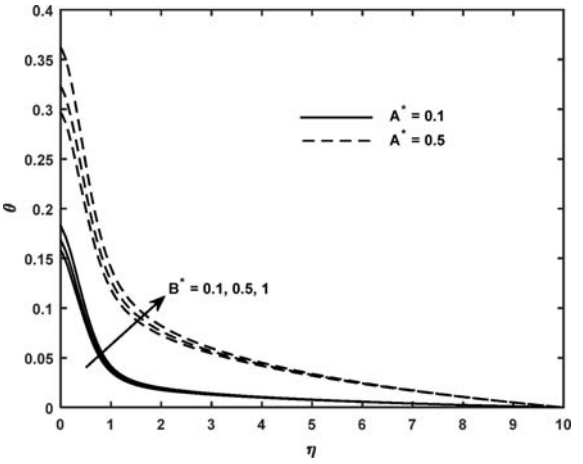

Fig. 8. Temperature profiles for different values of A^* and B^*

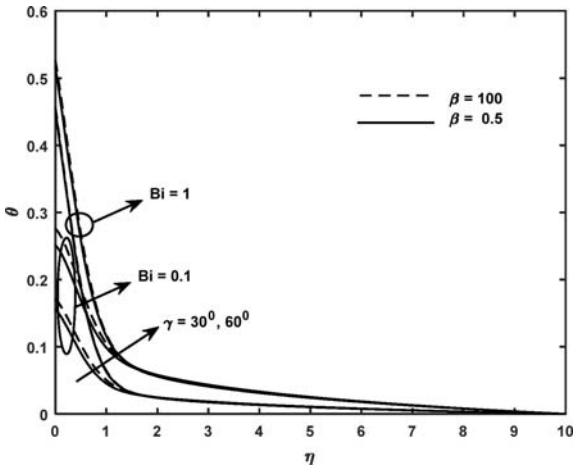

Fig. 6. Temperature profiles for different values of β, γ and $Bi > 0$

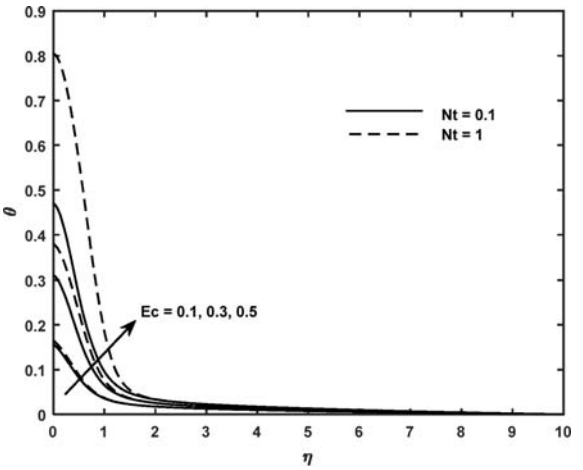

Fig. 9. Temperature profiles for different values of Ec and Nt

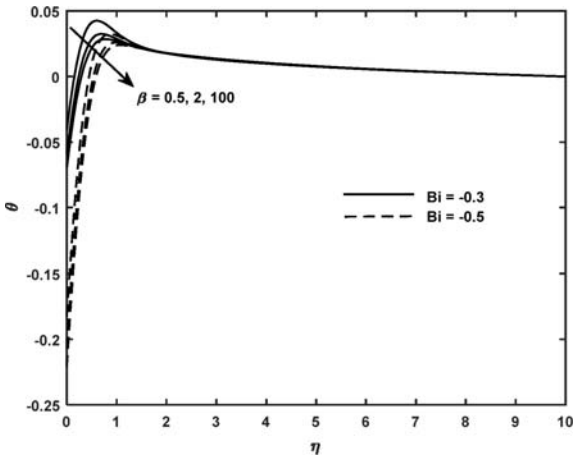

Fig. 7. Temperature profiles for different values of β and $Bi < 0$

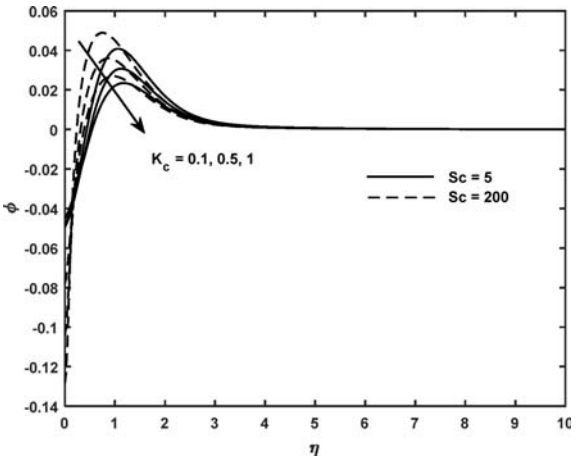

Fig. 10. Concentration profiles for different values of Sc and K_c

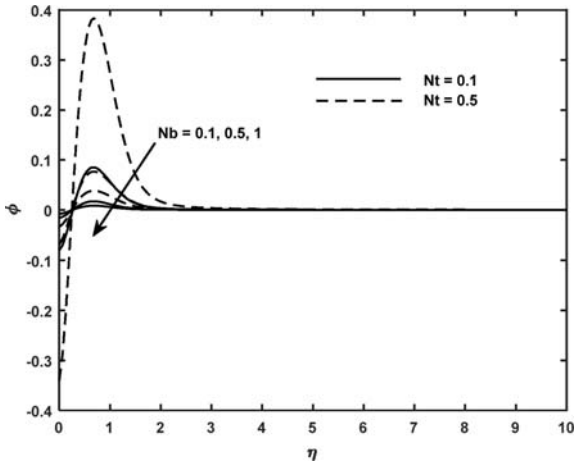

Fig. 11. Concentration profiles for different values of *Nb* and *Nt*

concentration profile shows an abrupt variation from -0.35 to 0.4 within a few layers near the plate for low values of Brownian motion parameter $Nb = 0.1$ and relatively high value of thermophoresis parameter $Nt = 0.5$. The fluctuation of concentration level decreases as *Nt*increases from 0.1 to 1.0. It is interesting to note that for high values of $Nb(Nb = 1.0)$ and low values of $Nt(Nt = 0.1)$, concentration level reduces smoothly. Therefore, coupling of low *Nb* with higher *Nt* is not desirable for solutal stability. It is also to note that an increase in *Nt* increases the concentration level for a fixed *Nb*.

Table 3 shows the negative values of skin friction and mass flux but positive values of heat flux. The negative values of the skin friction and mass flux at the surface indicate a downward drag and mass flows from the fluid to the plate respectively. Further, positive values of heat flux shows that the heat flows from the plate to the fluid. It is seen that an increase in Casson parameter (β), angle of inclination (γ) and ratio of stretching rate (λ) enhance the skin friction coefficient as well as surface heat flux $-\theta'(0)$ at the stretching sheet. This is in conformity with Reynolds analogy of skin friction and surface heat flux [45]. Further, it is to note that the parameters R, K_c, Sc, $A^*$and B^* have no significant effect on skin friction. On the other hand radiation parameter $(R)$and chemical reaction parameter (K_c) enhance the heat flux,

Table 3

Computation of $\left(1+\frac{1}{\beta}\right)f''(0)$, $-\left(1+\frac{4}{3}R\right)\theta'(0)$and $-\phi'(0)$ when. $M = Kp = Nb = Nt = Bi = 0.5, \Pr = 10, Ec = 0.1$.

λ	β	γ	R	Sc	Kc	A^*	B^*	$\left(1+\frac{1}{\beta}\right)f''(0)$	$-\left(1+\frac{4}{3}R\right)\theta'(0)$	$-\phi'(0)$
0.1	1	30°	0.1	1	0.1	0.1	0.1	−1.863182	0.307212	−0.162642
0.5	1	30°	0.1	1	0.1	0.1	0.1	−1.174292	0.354355	−0.187600
1.5	1	30°	0.1	1	0.1	0.1	0.1	1.339129	3.272751	−1.733986
0.5	2	30°	0.1	1	0.1	0.1	0.1	−1.016967	0.357798	−0.189422
0.5	3	30°	0.1	1	0.1	0.1	0.1	−0.958805	0.359119	−0.190121
0.5	3	45°	0.1	1	0.1	0.1	0.1	−0.936804	0.374789	−0.198418
0.5	3	60°	0.1	1	0.1	0.1	0.1	−0.879416	0.413926	−0.219137
0.5	3	60°	0.5	1	0.1	0.1	0.1	−0.879416	0.590325	−0.212517
0.5	3	60°	1	1	0.1	0.1	0.1	−0.879416	0.799035	−0.205466
0.5	3	60°	1	2	0.1	0.1	0.1	−0.879416	0.795908	−0.204662
0.5	3	60°	1	5	0.1	0.1	0.1	−0.879416	0.789917	−0.203121
0.5	3	60°	1	5	−0.1	0.1	0.1	−0.879416	0.787821	−0.202582
0.5	3	60°	1	5	−0.2	0.1	0.1	−0.879416	0.785795	−0.202061
0.5	3	60°	1	5	0.3	0.1	0.1	−0.879416	0.790756	−0.203337
0.5	3	60°	1	5	0.5	0.1	0.1	−0.879416	0.791004	−0.203401
0.5	3	60°	1	5	0.5	−0.3	0.1	−0.879416	0.905355	−0.232805
0.5	3	60°	1	5	0.5	−0.5	0.1	−0.879416	0.962524	−0.247506
0.5	3	60°	1	5	0.5	0.3	0.1	−0.879416	0.733820	−0.188696
0.5	3	60°	1	5	0.5	0.5	0.1	−0.879416	0.676628	−0.173990
0.5	3	60°	1	5	0.5	0.5	−0.3	−0.879416	0.698998	−0.179742
0.5	3	60°	1	5	0.5	0.5	−0.5	−0.879416	0.709242	−0.182376
0.5	3	60°	1	5	0.5	0.5	0.3	−0.879416	0.664391	−0.170843
0.5	3	60°	1	5	0.5	0.5	0.5	−0.879416	0.651370	−0.167495

indicating more amount of heat flows from the plate to the fluid and Scdecreases it. Thus, the effects of radiation and chemical reaction are important in augmenting the surface conditions in the presence of Newtonian cooling. Careful analysis reveals that mass flux increases with an increase in R, Sc, $A^*$and decreases with λ, βandγ. Therefore, it is remarked that mass flux acts adversely to those of heat flux and force coefficient at the plate in respect of λ, βandγ. These remarks serve as the guideline for obtaining the desired result.

4. Conclusions

From the current investigation the major finding are:

- Formation of inverted boundary layer is to be regulated by adjusting the relative shearing effect of plate and free stream.
- Increases in angle of inclination of magnetic field and thermal radiation ascribe to low flow rate and higher thermal diffusion.
- The slight change in Biot number leads to abrupt rise/fall in temperature in cases of Newtonian as well as Casson fluid (Figs. 6 and 7).
- Brownian motion has a reducing effect on concentration variation. Slight higher values of thermophoresis parameter leads to sharp rise in solutal concentration (Fig. 11).
- Increase in angle of inclination reduces the velocity in the boundary layer (Fig. 4).
- Concentration remains invariant in a layer close to the plate irrespective of heavier/lighter species (Fig. 10).
- In presence of Newtonian heating at the bounding surface the temperature of the nanofluid decreases with the higher values of Casson fluidity; this may have a therapeutic application to control the temperature of blood or any biological fluid.

Acknowledgements

The authors acknowledge their sincere thanks to the honorable unknown referees for their valuable comments.

References

[1] W. Ibrahim, B. Shankar, MHD boundary layer flow and heat transfer of a nanofluid past a permeable stretching sheet with velocity, thermal and solutal slip boundary conditions, Comput. Fluids 75 (2013) 1–10.

[2] D. Bhukta, G.C. Dash, S.R. Mishra, S. Baag, Dissipation effect on MHD mixed convection flow over a stretching sheet through porous medium with non-uniform heat source/sink, Ain Shams Engineering Journal 8 (2017) 353–361.

[3] A.A. Ahmed, The influence of slip boundary condition on Casson nanofluid flow over a stretching sheet in the presence of viscous dissipation and chemical reaction, Math. Probl Eng. (2017) 2–12.

[4] M. Mustafa, J.A. Khan, Model for flow of Casson nanofluid past a non-linearly stretching sheet considering magnetic field effects, AIP Adv. 5 (2015), 077148, https://doi.org/10.1063/1.4927449.

[5] T. Hayat, M. Bilal Ashraf, S.A. Shehzad, A. Alsaedi, Mixed convection flow of Casson nanofluid over a stretching sheet with convectively heated chemical reaction and heat source/sink, J. Appl. Fluid Mech. 8 (2015) 803–813.

[6] A.A. Afify, The influence of slip boundary condition on Casson nanofluid flow over a stretching sheet in the presence of viscous dissipation and chemical reaction, Math. Probl Eng. 2017 (2017), https://doi.org/10.1155/2017/3804751. Article ID 3804751, 12 pages.

[7] M. Abd El-Aziz, A.A. Afify, Effect of Hall current on MHD slip flow of Casson nanofluid over a stretching sheet with zero nanoparticle mass flux, Thermophys. Aeromechanics 26 (2019) 429–443.

[8] M.M. Rahman, I.A. Eltayeb, Radiative heat transfer in a hydromagnetic nanofluid past a nonlinear stretching surface with convective boundary condition, Meccanica 48 (2013) 601–615.

[9] W. Ibrahim, Nonlinear radiative heat transfer in magnetohydrodynamic (MHD) stagnation point flow of nanofluid past a stretching sheet with convective boundary condition, Propulsion and Power Research 4 (2015) 230–239.

[10] K. Swain, S.K. Parida, G.C. Dash, Effects of non-uniform heat source/sink and viscous dissipation on MHD boundary layer flow of Williamson nanofluid through porous medium, Defect Diffusion Forum 389 (2018) 110–127.

[11] M. Goyal, R. Bhargava, Simulation of natural convective boundary layer flow of a nanofluid past a convectively heated inclined plate in the presence of magnetic field, Int. J. Appl. Comput. Math. 63 (2018) 1–24.

[12] G.S. Seth, M.K. Mishra, A.J. Chamkha, Hydromagnetic convective flow of viscoelastic nanofluid with convective boundary condition over an inclined stretching sheet, J. Nanofluids 5 (2016) 511–521.

[13] D. Yadav, J. Wang, R. Bhargava, J. Lee, H.H. Cho, Numerical investigation of the effect of magnetic field on the onset of nanofluid convection, Appl. Therm. Eng. 103 (2016) 1441–1449.

[14] D. Yadav, D. Nam, J. Lee, The onset of transient Soret-driven MHD convection confined within a Hele-Shaw cell with nanoparticles suspension, Journal of the Taiwan Institute of Chemical Engineers 58 (2016) 235–244.

[15] D. Yadav, R.A. Mohamed, H.H. Cho, J. Lee, Effect of Hall current on the onset of MHD convection in a porous medium layer saturated by a nanofluid, Appl. Fluid Mech. 9 (2016) 2379–2389.

[16] D. Yadav, J. Lee, The onset of MHD nanofluid convection with Hall current effect, European Physical Journal Plus 130 (2015) 162–184.

[17] D. Yadav, The onset of longitudinal convective rolls in a porous medium saturated by a nanofluid with non-uniform internal heating and chemical reaction, J. Therm. Anal. Calorim. 135 (2019) 1107−1117.
[18] D. Yadav, The density-driven nanofluid convection in an anisotropic porous medium layer with rotation and variable gravity field: a numerical investigation, Journal of Applied and Computational Mechanics 6 (2020) 699−712.
[19] V.P. Rathod, S. Tanveer, Pulsatile flow of couple stress fluid through a porous medium with periodic body acceleration and magnetic field, Bulletin of the Malaysian Mathematical Sciences Society 32 (2009) 245−259.
[20] B.C. Krishnan, S.E. Rittgers, A.P. Yoganathan, Biouid Mechanics: the Human Circulation, Taylor and Francis, New York, NY, USA, 2012.
[21] G.W.S. Blair, An equation for the flow of blood, plasma and serum through glass capillaries, Nature 183 (1959) 613−614.
[22] N. Casson, Rheology of disperse systems, in: C.C. Mill (Ed.), Flow Equation for Pigment Oil Suspensions of the Printing Ink Type. Rheology of Disperse Systems, Pergamon Press, London, UK, 1959, pp. 84−102.
[23] E.W. Merrill, A.M. Benis, E.R. Gilliland, T.K. Sherwood, E.W. Salzman, Pressure-flow relations of human blood in hollow fibers at low flow rates, J. Appl. Physiol. 20 (1965) 954−967.
[24] S. Charm, G. Kurland, Viscometry of human blood for shear rates of 0-100,000 sec^{-1}, Nature 206 (1965) 617−618.
[25] P. Chaturani, R.P. Samy, Pulsatile flow of Casson's fluid through stenosed arteries with applications to blood flow, Biorheology 23 (1986) 499−511.
[26] M. Madhu, N. Kishna, MHD flow and heat transfer of Casson nanofluid over a wedge, Mechanics & Industry 18 (2017) 210.
[27] R. Kalaivanan, P. Renuka, N.V. Ganesh, A.K. Abdul Hakeem, B. Ganga, S. Saranya, Effect of aligned magnetic field on slip flow of Casson fluid over a stretching sheet, Procedia Engineering 127 (2015) 531−538.
[28] S. Jain, A. Parmar, Multiple slip effects on inclined MHD Casson fluid flow over a permeable stretching surface and a melting surface, International Journal of Heat and Technology 36 (2018) 585−594.
[29] B. Ganga, M. Govindaraju, A.K. Abdul Hakeem, Effects of inclined magnetic field on entropy generation in nanofluid over a stretching sheet with partial slip and nonlinear thermal radiation, Iran J. Sci. Technol. Trans. Mech. Eng. 43 (2019) 707−718.
[30] F. Mabood, K. Das, Outlining the impact of melting on MHD Casson fluid flow past a stretching sheet in a porous medium with radiation, Helyion 5 (2019), e01216.
[31] S.M. Ibrahim, P.V. Kumar, G. Lorenzini, E. Lorenzini, F. Mabood, Numerical study of the onset of chemical reaction and heat source on dissipative MHD stagnation point flow of Casson nanofluid over a nonlinear stretching sheet with velocity slip and convective boundary conditions, J. Eng. Thermophys. 26 (2017) 256−271.
[32] P.B.A. Reddy, Magnetohydrodynamic flow of a Casson fluid over a exponentially inclined permeable stretching surface with thermal radiation and chemical reaction, Ain Shams Engineering Journal 7 (2016) 593−602.
[33] C. Sulochana, N. Sandeep, V. Sugunamma, B. Rushi Kumar, Aligned magnetic field and cross-diffusion effects of a nanofluid over an exponentially stretching surface in porous medium, Appl. Nanosci. 6 (2016) 737−746.
[34] K. Swain, S.K. Parida, G.C. Dash, Thermal slip effect on MHD convective nanofluid flow over a vertical plate embedded in a porous medium, Eur. J. Eng. Educ. 20 (2018) 215−233.
[35] M. Senapati, K. Swain, S.K. Parida, Numerical analysis of three-dimensional MHD flow of Casson nanofluid past an exponentially stretching sheet, Karbala International Journal of Modern Science. 6 (1) Article 13 DOI: 10.33640/2405-609X.1462
[36] T. Hayat, M. Hussain, A. Alsaedi, S.A. Shehzad, G.Q. Chen, Flow of power-law nanofluid over a stretching surface with Newtonian heating, J. Appl. Fluid Mech. 8 (2015) 273−280.
[37] M. Uddin, O.A. Beg, W.A. Khan, A.I. Ismail, Effect of Newtonian heating and thermal radiation on heat and mass transfer of nanofluids over a stretching sheet in porous media, Heat Trans.-Asian Res. 44 (2015) 681, https://doi.org/10.1002/htj.21143.
[38] K. Ahmad, Z. Hanouf, A. Ishak, MHD Casson nanofluid flow past a wedge with Newtonian Heating, Eur. Phys. J. Plus. 132 (2017) 87, https://doi.org/10.1140/epjp/i2017-11356-5.
[39] I. Ullaha, S. Shafie, I. Khan, Effects of slip condition and Newtonian heating on MHD flow of Casson fluid over a nonlinearly stretching sheet saturated in a porous medium, J. King Saud Univ. Sci. 29 (2017) 250−259.
[40] J. Boungiorno, Convective transport in nanofluids, J. Heat Tran. 128 (2006) 240−250.
[41] S.K. Das, S.U.S. Choi, W. Yu, T. Pradeep, Nanofluids Science and Technology, Jhon Wiley & Sons, Inc., 2008, p. 262.
[42] H.D. Baehr, K. Stephan, Heat and Mass Transfer, second ed., Springer-Verlag Berlin Heidelberg, 2006, p. 117.
[43] T.R. Mahapatra, A.S. Gupta, Heat transfer in stagnation-point flow towards a stretching sheet, Heat Mass Tran. 38 (2002) 517−521.
[44] W. Ibrahim, B. Shankar, M.M. Nandeppanavar, MHD stagnation point flow and heat transfer due to nanofluid towards a stretching sheet, Int. J. Heat Mass Tran. 56 (2013) 1−9.
[45] H. Schlichting, K. Gersten, Boundary Layer Theory, eighth ed., Springer, p. 313.